

# Human Detection and Biometric Authentication with Ambient Sensors



Jack Andrews and Jia Li

## Abbreviations

AD	Alzheimer's disease
AI	Artificial intelligence
ANN	Artificial neural network
CM-PIR	Chest motion passive infrared sensor
CNN	Convolutional neural network
COTS	Commercial-off-the-shelf
CSI	Channel state information
DL	Deep learning
DWT	Discrete wavelet transform
ECG	Electrocardiogram
FFT	Fast Fourier transform
FN	False negative
FOV	Field of view
FP	False positive
GPR	Gaussian process regression
HAR	Human activity recognition
IDE	Integrated development environment
IOT	Internet of things
LSTM	Long-short term memory
MI-PIR	Motion induced passive infrared sensor
ML	Machine learning
PCA	Principal component analysis

---

J. Andrews (✉) · J. Li  
Department of Electrical and Computer Engineering, Oakland University, Rochester, MI, USA  
e-mail: [jackandrews@oakland.edu](mailto:jackandrews@oakland.edu)

PD	Parkinson's disease
PIR	Passive infrared
RELU	Rectified linear unit
RF	Radio frequency
RFID	Radio frequency identification
RNN	Recurrent neural network
RSSI	Received signal strength indicator
SGD	Stochastic gradient descent
TN	True negative
TP	True positive

## 1 Introduction

The geriatric population continues to increase and place a large burden on the healthcare systems worldwide. In 2019, there were 703 million people aged 65 or older across the globe. By 2050, this number is expected to double to an expected 1.5 billion people [1]. This increase in population is due to changes in lifestyle, the aging Baby Boomer generation, and increasing medical advancements, among other causes [2]. By 2030, the entire Baby Boomer generation will be older than 65 years of age and at that point, for the first time in the history of the United States, elderly people will outnumber the child generation. As evidence, by 2034, there will be 77 million people 65 years and older compared to 76.5 million people under the age of 18 [3]. The population older than 65 years of age currently accounts for 35% of all medical spending in the United States, indicating how the change in the population demographics may further impact the medical spending across the United States federal funding and health systems [4]. Many of these individuals are admitted to the hospital system for assistive care, as many normal activities can no longer be performed alone due to potential falls and memory loss [2].

Neurodegenerative diseases include dementia, Alzheimer's disease (AD), Parkinson's disease (PD), among various others. Largely due to these diseases, geriatric populations require additional assistance from a caregiver or admission to a long-term care facility site. Neurodegenerative diseases are complex in their pathophysiology, as some diseases cause memory and cognitive impairments, where others effect speaking and gait ability [5]. Due to this progressive degeneration in motor stability and memory, many of those that suffer from neurodegenerative diseases are prone to falls and memory loss effects [6]. For an insight into the number of people who suffer from neurodegenerative diseases in the United States, in 2015, five million suffered from AD and one million suffered from PD [7]. Aging individuals, especially those suffering from neurodegenerative diseases, generally require assistive care for safe long-term living.

For safe and secure living in these presented populations, a caregiver or hospital stay is often required, which causes financial burdens on both the families and the healthcare system. With an increasing number of people in these categories, the financial burdens will continuously increase. There exists a need for remote monitoring systems to aid caregivers and hospital systems to allow for greater

independence and alleviate the burden of these populations on the healthcare system. There exist many proposed systems for remote monitoring of geriatric populations in at-home environments in current research and in industry. Proposed solutions often utilize ambient sensors and artificial intelligence (AI) algorithms for accurate monitoring of the environment. Many of these systems rely on video-based modalities which raise privacy concerns for the monitored person. In addition, many systems rely on expensive hardware or difficult set-up with multiple sensors deployed throughout the home. Some systems utilize active sensors that raise some energy and health concerns as well. An accurate, non-intrusive, passive, inexpensive, and ubiquitous monitoring system for an at-home environment could solve these aforementioned shortcomings.

The utilization of ambient sensors and AI extends from the need of human monitoring applications to security and biometric authentication applications. With the advent of the internet of things (IoT), there exists a need for an enhanced sense of security of personal data. IoT specifically refers to the interconnection of the devices used in everyday life including kitchen items, beds, phones, cars, and televisions [8]. IoT is expected to continue to increase as well, as in 2030 an estimated 500 billion devices will be connected to the Internet [9]. The security of the ever-increasing number of connected devices in our daily life remains a challenge, as potential adversaries can take advantage of personal data, as well gain entrance to medications or personal belongings [8]. To protect the security of IoT devices, passwords are often utilized, but they can often be forgotten or stolen. Facial recognition and fingerprinting technologies have become popular and have reached consumer IoT devices as alternatives to written passwords, as seen in common Apple products. However, these too can be unreliable and forged [10, 11]. For instance, once a fingerprint is stolen or retrieved from a touched surface, the fingerprint will forever be compromised [12]. A whole sector of security using biological characteristics is referred to as biometrics and can be used for authentication and identification of individuals for increased security of IoT devices. Where passwords can be forgotten or stolen, biometrics are unique to one individual person and are more difficult to replicate [8].

Biometric authentication refers to the use of a unique biological quality to confirm one person's identity against all other potential adversaries, while biometric identification classifies every individual in the dataset as unique. Common biometrics include previously mentioned fingerprints and facial recognition with additional unique characteristics including iris, gait, and voice. These biometrics are used to enhance the security of IoT devices, in comparison to written passwords or PIN numbers. Biometrics can be captured via non-contact sensors, such as in the case of cameras for facial recognition. Cameras, however, raise privacy concerns to the end-user. Therefore, a non-contact sensor for biometric authentication that alleviates the privacy intrusion to the end-user is seen as a superior modality for this purpose. With deep learning (DL), the collected biometrics from a non-contact sensor can be learned to differentiate a verified user against all other potential adversaries. To summarize, there exists a need for a secure, accurate, non-contact, and non-intrusive biometric authentication system to further enhance the security of IoT devices. Heart-related biometrics are growing in popularity, have shown promise as

reliable for biometric authentication and identification systems, and could fill these mentioned shortcomings.

Various ambient sensors for non-contact sensing have been proposed for these applications including cameras, thermal sensors, depth sensors, and passive infrared (PIR) sensors. With the need for non-contact human monitoring and biometric authentication systems in mind, PIR sensors are inexpensive, commercial-off-the-shelf (COTS) components that are often utilized in monitoring and security applications. PIR sensors work by identifying the change in infrared radiation across its field of view (FoV) which is detected by the internal pyroelectric elements with alternating polarity. With everything above absolute zero temperature emitting some level of infrared radiation, theoretically any object in motion across a PIR sensor will be detected. As a result, human subjects in motion across a traditional PIR sensor will be detected. The major known drawback to PIR sensors, however, is the lack of reliable and accurate detection of stationary human subjects. For accurate use in human monitoring and biometric authentication situations, the inability to detect stationary human occupants will first have to be addressed.

To combat these mentioned drawbacks of human detection and biometric authentication systems, ambient sensors and AI have been proposed. Likewise, ambient signals have also garnished interest for non-contact monitoring including the likes of radio frequency (RF) and WiFi channel state information (CSI) for this purpose. DL algorithms including artificial neural networks (ANN), recurrent neural networks (RNN), and convolutional neural networks (CNN) have been utilized for learning of the sensor data for human detection and biometric authentication purposes. In our work, we propose using a PIR sensor as the ambient sensor with various statistical learning algorithms for human detection and biometric authentication classifications.

To address human detection and biometric authentication classifications via a single PIR sensor modality, we introduce and propose two novel systems in this work . . .

1. Motion induced PIR sensor (MI-PIR)
2. Chest motion PIR sensor (CM-PIR)

Both systems are proposed to address the noted major known drawback of PIR sensors, which is the inability to reliably detect stationary human subjects [13, 14]. For MI-PIR, we extend the capabilities of this system from occupancy count estimation, relative location classification, and human target differentiation in one environment to precise indoor localization and human activity recognition (HAR) in two different ambient environments. For CM-PIR, we reintroduce the initial results of the biometric authentication system based on the chest motion data collected from 16 subjects at nine different home environments [14]. Human monitoring and biometric authentication via non-contact sensors and AI overall proves to have direct applications in medicine and healthcare as identified in assistive care living and security of private medical data from IoT devices. Accurate non-contact sensing systems will allow for long-term living in the elderly populations and more secure IoT devices, respectively.

## 2 Related Work

For accurate comparison of the two novel systems proposed in this work, many related systems will be introduced. For stationary human presence detection using PIR sensors, various solutions have been introduced, primarily those that rely on an optical shutter for accurate detection. Various additional ambient sensor modalities have been proposed for human monitoring and biometric authentication classifications that will also be highlighted in this section.

### 2.1 PIR Sensors

PIR sensors function by detecting the change in infrared radiation across its FoV. For binary PIR sensors, the change in infrared radiation will result in a “1” for a detected human subject and a “0” for no human subject detected. With infrared radiation being the resultant of temperatures greater than absolute zero temperature, other objects could potentially trigger a binary PIR sensor. For example, animals walking across the FoV of the PIR sensor, as well as a potential ball, car, or other object, could theoretically cause a false positive for a binary PIR sensor. When human bodies radiate infrared radiation from their body, there is a significant energy loss. The infrared radiation lost from a human body can be modeled by Eq. (1) below, which relates the energy loss from a blackbody (T) with its surroundings ( $T_s$ ). In Eq. (1), the total power radiated from the human body ( $W_{tot}$ ) is represented by this energy loss ( $T^4 - T_s^4$ ) multiplied by the total surface area of the human in question (S) and the Stefan-Boltzmann constant ( $\sigma_{SB}$ ) [15]. Eq. (1) proves the ambient environmental dependence on the infrared radiation of a human subject.

$$W_{tot} = S\sigma_{SB} \left( T^4 - T_s^4 \right) \quad (1)$$

Analog PIR sensors output the voltage readings of the detected infrared radiation from a PIR sensor instead of the binary output, where an object in motion across the FoV will trigger a sinusoidal swing for the positive and negative terminals of the pyroelectric elements indicating human presence. For a typical human in motion, this will cause a swing to the maximum voltage and back to the minimum voltage; however, this sinusoidal swing is dependent on the mentioned ambient environment, and the motion and distance of the human subject. As a result, DL was proposed as a solution to learn from the varying outputs of the analog PIR sensor for various classifications including differentiating ambient environments, occupancy counts, human locations, and human subjects.

The FoV of a PIR sensor is generally expanded with the addition of a Fresnel lens. The Fresnel lens works to distribute the FoV of a PIR sensor into many evenly spaced fan-shaped zones with alternating polarities [16]. The Fresnel lens also works to expand the FoV of the PIR sensor by focusing the thermal image on



**Fig. 1** Novel MI-PIR system including the (a) the Panasonic AMN24112 and (b) the full design

the internal elements, which converts the thermal energy of the image into heat. Varying PIR sensors use different Fresnel lens and thus, there exist different FoV ranges for each PIR sensor [17]. In our work, we utilize the Panasonic AMN 24112 PIR sensor with analog output as identified in Fig. 1(a). The Fresnel lens on the Panasonic AMN 24112 PIR sensor expands the FoV to a recorded horizontal  $93^\circ$  and vertical  $110^\circ$ .

As stated, PIR sensors rely on a change in infrared radiation for accurate detection of a human subject. Due to this, stationary human subjects often go undetected and result in a major drawback to the deployment of PIR sensors in monitoring and security applications. To combat this issue, multiple designs have been proposed for the accurate and reliable detection of stationary subjects with a PIR sensor. Initial designs utilize additional hardware with the inclusion of an optical shutter to periodically chop the FoV of the PIR sensor to artificially cause a motion change for the stationary human subject [18]. In addition, Ya Wang's group at Texas A&M has been awarded a one-million-dollar grant to enhance an optical shutter design for more reliable energy management solutions. The goal of the project is the development of an advanced, low-cost occupancy sensor named SLEEPIR that enhances industry PIR sensors for more accurate detection [19–24]. In our work, we propose two varying systems for stationary human subject detection using a PIR sensor. MI-PIR, the first design, classifies room occupancy through a 36 s rotation to induce the motion necessary for human detection. CM-PIR, on the other hand, relies on the chest motion from the heart to detect stationary subjects. These two designs will be presented further throughout this chapter.

## 2.2 AI

AI refers to the use of a computer to mimic human knowledge. The origin of AI can be traced to the 1950s, but overall, the field of AI is still premature [25]. Machine learning (ML) is a subset of AI and refers to a computer's ability to train itself without being explicitly told how to do so. DL is a subset of ML and is referred to

as a type of neural network, one that trains itself through multilayered networks of data operation [26]. DL is an immensely powerful tool that can automatically learn from unstructured datasets, learning the slight variations that exist between the data samples while functioning like the neurons in the brain. AI is consistently used with non-contact ambient sensors to learn from the complex scenarios that exist within these datasets. There exist various algorithms utilized for this purpose including ML algorithms such as Random Forest, Support Vector Machine, and Gaussian process regression (GPR) and DL algorithms including artificial neural networks (ANN), recurrent neural networks (RNN), and convolutional neural networks (CNN). In our work, we utilize GPR for precise indoor localization and ANN, RNN, and CNN as comparison for each other classification.

A Gaussian process can be completely defined by its mean and covariance function and is defined as a collection of random variables, with any finite number of which have (consistent) joint Gaussian distributions. GPRs remain powerful tools due to its probabilistic methods of predicting the output mean and variance conditional on a specific input at a specific instance of time. GPR models differ from classification models in that a location estimation can be predicted from GPR models, whereas a classification algorithm outputs classification results. Various parameters in the implementation of these models are to be optimized, including the kernel function [27]. There exist a variety of kernels that are often used in implementation of GPR models including Squared Exponential, Periodic, and Matern, just to name a few [28]. Performance of these models are often indicated with the quantification of the mean squared error (MSE) which is shown in Eq. (2).  $y_j$  refers to the observed values,  $y(x_j)$  refers to the predicted values, and  $N$  is the number of data points in the training set [15].

$$MSE = \frac{1}{N} \sum_{j=1}^N (y_j - y(x_j))^2 \quad (2)$$

In terms of DL, ANNs are the most basic feedforward approaches to learning and are used for a variety of tasks including pattern recognition, image recognition, and natural language processing. ANNs are composed of multiple dense layers that feedforward and do not learn recursively [29]. RNNs, on the other hand, are a recursive approach to learning, having an internal memory and making them particularly useful for time-series data classifications. RNNs work by taking time and sequence into account, where the output of one layer will in turn be fed to the input of a previous layer [30]. This approach to learning suffers from the vanishing gradient issue and must be overcome with the use of long-short term memory (LSTM) units in the application [31]. CNNs are often utilized for image recognition tasks as their architecture is designed specifically for this purpose. CNNs consist of multiple layers including fully connected layers, max pooling layers, convolutional and non-linearity layers [29].

Adequate reporting of these algorithms is essential, and the metric used for performance measurement often varies based on the classification task at hand.

Broadly, Explainable AI is a new field that is based on assessing the performance of ML algorithms to alleviate the black-box stigma surrounding AI [32, 33]. In general cases, reporting of the performance is completed with metrics such as accuracy, F1 score, area-under-the-curve, precision, or recall. Accuracy refers to the number of correct predictions that the statistical modeling labeled correctly divided by the total number of predictions that were made. Classification reports are often presented as a table that includes accuracy and various additional metrics. Visually, reporting of the confusion matrices, visual data, and training and testing curves also aids in the understanding of the performance. Confusion matrices visually identify the true positive (TP), true negative (TN), false positive (FP), and false negative (FN) of each classification by presenting the number of testing samples that were correctly and incorrectly classified. The confusion matrix provides actual values and expected values on the axes, and the resulting internal values are indicative of the number of correctly labeled samples in either normalized or unnormalized form. For the purposes of human detection and biometric authentication, we primarily rely on accuracy, visual data, classification reports, and confusion matrices to present the performance of the algorithms used.

### 2.3 *Human Monitoring*

There exist various methodologies for human monitoring purposes using ambient sensors and AI in related work. Ambient sensor modalities in literature that have been utilized for human monitoring purposes include microwave sensors, thermal sensors, and optical sensors. In terms of utilizing microwave sensors for human monitoring purposes, multiple sensors were distributed in the environment for multi-person HAR using a 3D-CNN for learning [34]. Using solely ambient thermal sensors and ML algorithms, detection of human presence was shown to be 100% accurate, with additional classifications of occupancy count estimation and HAR proving 100 and 97.5% accurate, respectively. The position of the thermal sensors affected the results of this work, with three sensors being deployed in this work, each having a horizontal FoV of 125° ([35]). An infrared active imaging system and a CNN learning model were utilized for human detection with a specific application to instances of home fires in another related work [36]. Further, image sensors were deployed iteratively for occupancy counts in a large exhibition hall with optical sensors deployed at entrances and exits. Learning of the occupancy counts in each zone of the exhibition hall was accomplished with an RNN with LSTM units [37].

Worth mentioning are the commonality of utilizing ambient signals for human monitoring purposes. In terms of leveraging ambient signals for human monitoring purposes, related works have utilized passive radio frequency identification (RFID) tags, passive RF signals, active RF signals, and Wi-Fi CSI. For example, a *SmartWall* composed of multiple passive RFID tags were utilized for localization and HAR purposes [38]. Similar in usage of passive RF-based signals, our group has published work on utilizing passive RF signals for human detection in residential

and automobile environments. This work utilizes principal component analysis (PCA) for dimensionality reduction, recursive feature elimination with logistic regression, and ML algorithms for accurate human detection [39]. More common in literature are the use of active band RF signals for human monitoring applications. State-of-the-art research performed by the MIT CSAIL group has shown the efficacy of such approach, through the classification of human activities and their respective locations even through walls and occlusions [40–42]. Further, a millimeter-wave radar system was proposed for its low-cost approach in the proposed *RadHAR* system for HAR of five different exercise activities using a CNN-LSTM learning model [43]. Wi-Fi CSI via IoT devices can also prove successful at human monitoring, for HAR was shown to achieve 97.6% accuracy using a novel DL framework which was coined AE-LRCN [44].

In addition to the success of the previously mentioned sensor modalities, PIR sensors also have proven successful in human monitoring applications. Through a sensor fusion of PIR sensors and camera modalities, *HeteroSense* obtained accurate classifications for presence, occupancy count, trajectory or tracking, and basic multiclass activity recognition [45]. In *HeteroSense*, stereo-vision cameras are placed at entrances and multiple PIR sensors are deployed throughout the indoor environment for accurate classification. Sensor fusion with PIR sensors is popular in human monitoring applications, as the binary output of the PIR sensor is used for trajectory detection of the human subject and the other sensor modality is traditionally used for more continuous monitoring in sedentary moments. Another sensor fusion system can be seen with a geriatric monitoring application utilizing eight PIR sensors in a mock apartment environment with one wearable device connected to the thigh of the monitored subject. In this instance, a Bayesian particle filtering sensor fusion algorithm is applied for greater indoor localization accuracy [46]. In a similar sense, PIR sensors were deployed for early detection of dementia based on classification of travel patterns with a CNN learning model [47]. In terms of HAR using only PIR sensors, in the proposed system *ALPAS*, four activities completed on a sofa were classified with a F-measure of 57% using only two analog PIR sensors [48].

Although indoor localization has been classified through DL algorithms, indoor localization via GPR models is a common approach to localization. Regression is seen as superior in terms of indoor localization as estimation of testing data can apply to new coordinate systems in the environment of interest. One example of such an approach for indoor localization is coined *DeepMap*, a deep Gaussian process for indoor radio map construction and indoor localization [49]. The received signal strength (RSS) of Wi-Fi signals are used as fingerprints in this related work, for which the deep Gaussian process is fed and learns from these RSS values and their respective coordinates for accurate human localization. Similarly, authors in related work utilized Wi-Fi received signal strength indicator (RSSI) fingerprinting data for indoor localization via GPR, in which a CNN was also deployed to learn the features from RSSI data before being fed into the GPR model. The RSSI fingerprints were pre-processed in this case to represent images, in which such a designed process in this work of CNN + GPR with a Matern kernel proved superior to the k-

Nearest Neighbor algorithm in compared work [50]. A novel multi-person tracking framework was proposed utilizing a GPR observation model through a transfer learning approach. The prediction from the Kalman Filter feeds into the GPR model to estimate the targets' location and then the output of the GPR model is then used as the measurement input into the Kalman Filter [51]. In a work completed by our research group, the offline training phase is modeled by a 3D point cloud and the developed GPR model learns from the RSS of Wi-Fi signals for matching completed during the online stage. This methodology proved accurate for indoor localization on an iOS platform [52].

For elderly monitoring, indoor localization and HAR are two applications that significantly aid in greater independence for the monitored person. The caregiver and hospital system will be able to check on the status of the aging individual and monitor potentially harmful activities without being physically in their presence. Common in many systems designed specifically for the elderly and neurodegenerative populations is the detection of fall events, as fall events are the leading cause of death in these populations [53]. Many fall detection systems rely on sensors embedded in wearable devices for accurate detection of fall events, yet there exist ambient sensing systems that are designed for accurate classification of fall events. One such instance is proposed where the authors used a video-based detection system [54]. Human poses in this related work are used as features that are fed into a CNN for feature extraction and classification, achieving high sensitivity and specificity in comparison to other fall detection systems using raw RGB data. In neurodegenerative monitoring, an ultra-low-power radio signal device coined *Emerald* was developed and subsequently monitored seven PD patients passively with a focus on gait, home activity, and time in bed [55].

With the presentation of related systems based on ambient sensors and statistical learning algorithms, one can determine the shortcomings in these various systems. For example, those systems that rely on video-based detection are prone to privacy concerns that limit its long-term usage in at-home monitoring systems. In addition, video-based systems can be expensive for widespread deployment in assistive care facilities. Some systems with active sensors are prone to health and energy concerns, such as in the case of active RF signals. Some systems that deploy specific sensors, or PIR sensors in the traditional sense, are limited by the small FoV, requiring multiple sensors deployed in the monitored environment. Terminal devices used in sensor fusion with PIR sensors require the user to remember to consistently wear the device, causing intrusion on the monitored human subject. Therefore, as mentioned, there exists a need for inexpensive, non-intrusive, accurate, and expanded ambient sensing systems towards the reliable monitoring of aging individuals. A PIR sensor that extends the FoV to monitor an entire environment and accurately detect stationary human subjects could potentially fill the gaps in this related work.

## 2.4 *Biometric Authentication*

Biometric authentication methodologies vary in the modality and the metric used for classification. For instance, wearable devices have utilized biometric authentication methodologies towards the goal of secure and implicit authentication of these devices. One instance of this was presented with the usage of hybrid biometrics for biometric authentication, using calorie burn and metabolic equivalent of task (MET) metrics during sedentary and non-sedentary stages [56]. In terms of ambient, non-contact sensing for authentication purposes, many systems rely on camera modalities, such as in the case of imaging of fingernail plates and finger knuckles. Utilizing rank-level fusion of the two image features, the proposed system achieved 100% accuracy from a database containing 890 total images of 178 volunteers [57]. These examples highlight the variations in methodologies for the common biometric authentication goal. Towards biometric authentication systems that are less prone to forgery and indicate living human presence, heart-related biometrics have garnered much attention in recent years.

Electrocardiogram (ECG) is a measurement of the electrical activity of the heart, which is generally dependent on surface electrodes. The waveforms that exist in an ECG signal include the P, Q, R, S, and T waves, which are indicative of repolarization and depolarization of various parts of the heart [15, 58]. These collected ECG signals are commonly deployed for biometric identification and biometric authentication purposes based on the unique QRS complex that exists for each heartbeat of the ECG signal. More generally, these methods for biometric identification and authentication are based on the physiological background that everyone has a unique heartbeat due to the variations in opening and closing of valves and varying sizes and shapes of each heart. Common methodologies for biometric authentication and identification with ECG signals rely on DL to learn the slight variations that often exist between the QRS complexes. For example, a CNN was deployed to intrinsically learn the features contained within the MIT-BIH database of ECG signal data resulting in a 99% accurate biometric identification system. The novelty of this proposed system is such that this methodology eliminates the usual time-extensive manual feature engineering process [59]. Likewise, another biometric identification system based on ECG signal data was proposed, where in this instance, the novelty was based on the QRS-resampling strategy that was proposed to handle the variations in heart rate. This QRS-resampling strategy with a PCANet DL architecture allowed for a 94.4% accurate identification system that is robust to heart rate variability [60]. Towards the goal of improving the generalization ability of ECG identification systems, a cascaded CNN was proposed for biometric identification of ECG signal data in another related work, where the F-CNN is used for feature extraction and M-CNN is used for classification [61]. Although accurate enough to identify every individual included in the dataset, ECG signals require contact with the user and are reliant on expensive hardware. To improve biometric systems for everyday usage, such as in the case of IoT, capturing heart-related signals with more advantageous sensor modalities is examined.

Collecting an accurate and informative heart rate signal is more difficult with non-contact sensors. A few solutions, however, have been proposed in recent years on this topic. ECG signals can now be captured via wearable devices such as an Apple Watch or in the case of capacitive coupled electrodes embedded within clothing. In the latter example, the researchers proposed methods for artifact reduction in such non-contact ECG monitoring examples, showing that their proposed empirical wavelet transform with traditional wavelet transform approach was successful at reducing motion artifacts and restoring the QRS complexes [62]. Moreover, the breathing pattern and respiratory rate (RR) has been shown to be accurately quantified via RGB cameras [63]. Collecting these signals would allow for a non-contact, heart-related biometric system; yet, collecting RGB images raises privacy issues that should be avoided for a long-term monitoring solution. In more recent work, the WiFi CSI ambient signals have shown success at estimating the RR through high-resolution spectrogram-based CSI features for a COVID-19 monitoring application [64]. A PIR sensor would address the shortcomings of other sensor systems and fit the needs of a long-term monitoring solution. Presented in related work is a PIR sensor that accurately estimates the resting heart of 30 subjects using a novel acceleration filter that is presented in Eq. (3) [65]. The magnitude of the heart-rate signal is much greater than the respiratory signal for the applied acceleration filter, allowing for accurate resting heart rate estimation from a PIR sensor in this related work. The novel acceleration filter in Eq. (3) computes the second derivative with a convolving triangular window and simple Lagrange low pass filter to the raw PIR analog sensor data.

$$g_2' = [1 \ 4 \ 4 \ -4 \ -10 \ -4 \ 4 \ 4 \ 1] \quad (3)$$

This acceleration filter in Eq. (3) is utilized and included as a feature for biometric authentication in our work. In their methodology, subjects sat 1 m away from the PIR sensor while remaining motionless, and their chest motion was collected at a 10 Hz sampling rate [65]. Showing to be successful at extracting the heart rate of individuals with a PIR sensor, we follow a similar methodology in our CM-PIR system. In comparison to a proposed system using a PIR sensor for biometric authentication, a system coined *Cardiac Scan* utilizes a DC-coupled continuous-wave radar for the authentication of 78 subjects at one common location. The cardiac motion acts as a biometric in this case, showing to be 98.61% accurate using a SVM algorithm with RBF kernel [66]. This non-contact biometric authentication system for an IoT device indicates the similarity to our proposed CM-PIR system.

### 3 Motion Induced PIR

MI-PIR was previously introduced as a novel method for stationary human presence detection using one analog PIR sensor and an ANN DL model [13]. Additionally, MI-PIR consists of a robotic actuator, a platform, a thermal insulator, a microcon-

troller, and a PC. The complete set-up of MI-PIR is included in Fig. 1(b). The thermal insulator is made of cardboard, as this material was shown to accurately block the infrared radiation detected from the movement of the robotic actuator. A more long-term material will be developed and replace the cardboard in this system in a future model. The thermal insulator sits on the platform and subsequently the robotic actuator. The robotic actuator used in the MI-PIR design is the Dynamixel MX-28, while the platform is a Hokuyo UTM-30LX-EW which serves no other purpose than to be used as a flat surface for the thermal insulation material. The Elegoo Uno R3 microcontroller connects to the Panasonic AMN24112 PIR sensor for data conversion and transmission to the PC. This full MI-PIR design classifies a room occupancy and related parameters every 36 s due to the 26 s forward motion and the 10 s backward motion to complete one full cycle.

In our initial work, MI-PIR was extended to classify three additional occupancy parameters on top of stationary human presence detection, which included occupancy count estimation, relative location classification, and human target differentiation. New in this work is the addition of precise indoor localization and HAR in both an office environment and residential environment. We utilize a GPR model for precise indoor localization achieving  $493.7 \text{ cm}^2$  MSE in an office environment with multiple users and  $426.4 \text{ cm}^2$  MSE for Student 1 only of Table 1. An RNN model with LSTM units for HAR achieved 100% accuracy in the office environment for classifying activities of Student 1 only. In the residential environment, the GPR model achieved  $131.4 \text{ cm}^2$  MSE for precise indoor localization of one individual and the RNN architecture achieved 98% accuracy between six total labels for HAR. The data collection, pre-processing, and results of the MI-PIR system will be fully addressed in this section.

### 3.1 Ambient Environments

The office location is in Dodge Hall, an academic office building on the campus of Oakland University in Rochester, Michigan, USA. This office location consists of five different PC locations labeled as “Location (L1)” through “Location 5 (L5)”, where MI-PIR is placed for data collection at Location 1. In addition, the office location is split into three different walking paths for HAR data collection. The office location is 5.18 m in length and 3.96 m in width and is only accessible by key access. As a result, student researchers are of those with access and are commonly using the office space. Each researcher in the lab has a common workstation, but due to fluidity in the student researchers, there does exist some variation in the student locations. The office location has been modeled and is presented below in Fig. 2. L1 through L5 label the locations of student researchers and W1 through W3 label walking paths in this figure.

In relation to the office location, a residential location is more indicative of an elderly monitoring situation, and thus the MI-PIR system was additionally tested in an apartment bedroom. The residential environment is 4.57 m in length and

**Table 1** MI-PIR data collection in the office space location for each of the five classifications and two regression models. The number label used for DL, along with the real label and available samples for a 36 s rotation time is included

Classification	Number label for ML	Real label	Available samples
Room classification	0	Unoccupied	854
	1	Occupied	2803
Occupancy count estimation	0	No people	854
	1	One person	1936
	2	Two people	702
	3	Three people	165
Relative location classification	0	Unoccupied	854
	1	Location 1	174
	2	Location 2	1240
	3	Location 3	153
	4	Location 4	369
	6	Locations 1 and 2	105
	10	Locations 2 and 3	44
	11	Locations 2 and 4	100
	12	Locations 2 and 5	250
	15	Locations 4 and 5	203
	23	Locations 2, 3, and 5	138
	24	Locations 3, 4, and 5	21
	25	Locations 2, 4, and 5	6
Human target differentiation	0	Unoccupied	854
	1	Student 1	1936
	2	Students 1 and 2	32
	3	Students 1 and 3	181
	4	Students 1 and 4	386
	5	Students 1 and 5	103
	6	Students 1, 4, and 5	98
	7	Students 1, 3, and 5	46
Indoor localization	(250, 10)	Unoccupied	7136
	(415, 70)	Location 1	279
	(415, 265)	Location 2	1883
	(250, 265)	Location 3	356
	(80, 265)	Location 4	699
	(50, 60)	Location 5	618
Indoor localization— Student 1	(415, 70)	Location 1	174

(continued)

**Table 1** (continued)

Classification	Number label for ML	Real label	Available samples
	(415, 265)	Location 2	483
	(250, 265)	Location 3	153
	(80, 265)	Location 4	369
Activity recognition— Student 1	0	Unoccupied	191
	1	Sitting	102
	2	Walking	101

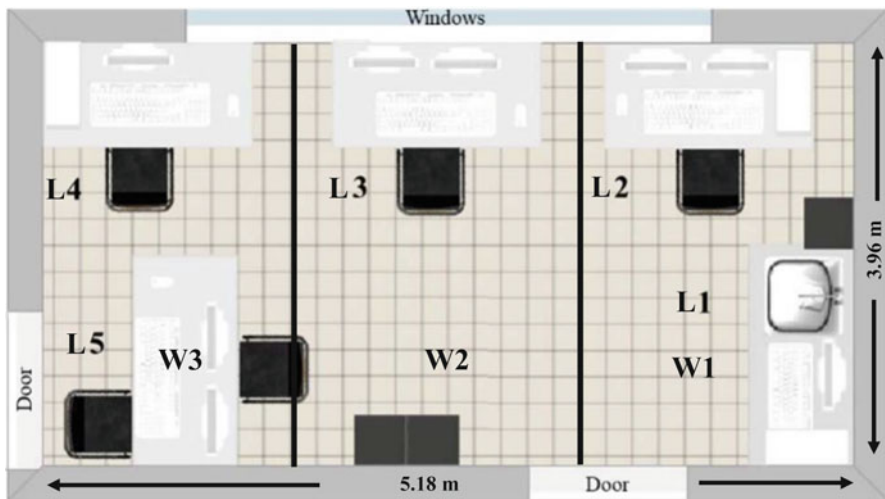


**Fig. 2** The model of the office space. “L1” through “L5” indicate the five stationary locations in the office space and “W1” through “W3” indicate the three walking paths during the HAR data collection. MI-PIR is located on the counter at L1

3.65 m in width, just smaller than that of the office environment. In this location, a relative location classification and HAR classification are completed. In addition, a precise indoor localization is applied to identify the results of estimating a human occupant’s position in a residential environment. This specific residential environment is modeled in Fig. 3. This apartment model indicates the locations for which each activity is completed, specifically presenting Activity 1 (“A1”) of “Working at the Desk” at Location 2 (“L2”) in Fig. 3. Further, Location 1 on Fig. 3 (“L1”) indicates the locations of Activity 2 (“A2”) and Activity 3 (“A3”), “Laying on the Ground” and “Exercising on the Ground”, respectively. Location 3 is located at the bed for which Activity 4 (“A4”) and Activity 5 (“A5”) are completed of “Watching TV on Bed” and “Sleeping on Bed”, respectively.

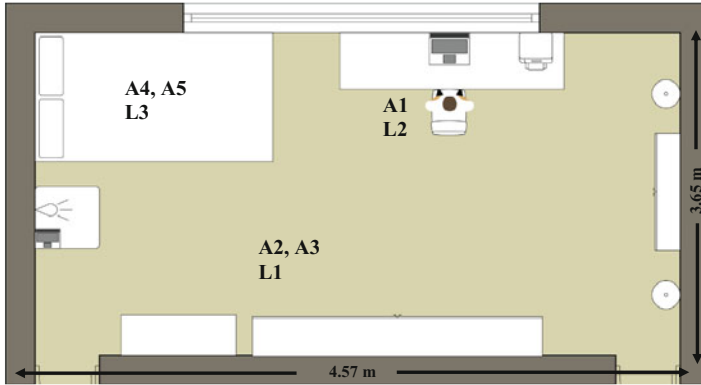


**Fig. 3** Model of residential environment data collection. MI-PIR is located next to the bed, indicated by the outward signals

## 3.2 Data Acquisition

For data acquisition, MI-PIR scans the room every 36 s in a 130° motion, including both a forward and backward trajectory. As a result, the horizontal FoV is increased from 93 to 223° with the MI-PIR design. Data was collected at a 10 Hz sampling rate. Each data sample is synced to match the ambient environment e.g., each data collection sample starts with the MI-PIR system pointing in the farthest east direction. For unoccupied data collection, an additional 36 s is included to copy the data that matches the accurate situation. The data collected was copied from the serial monitor of the Arduino integrated development environment (IDE) and then converted to a CSV format, where it was cleaned and manually labeled. Each data sample includes the labels for learning and the time for each classification. The data samples are finally sent to their respective folders for each classification.

### 3.2.1 Office Environment

Office data collection for stationary human presence detection, occupancy count estimation, relative location classification, and human target differentiation was completed between August to December of 2019. This covered the change in the summer semester to the fall semester on campus, allowing for variations in the student researchers and their usual locations in the office environment. The ambient environment in the data collection varied due to the sunlight changes between seasons that existed with the open windows in the office. These changes between locations and ambient environments allow for a more robust monitoring system. Precise indoor localization via GPR is based on the same data collection; however, data collection for the “walking” label of HAR was collected in March by Student 1. HAR in this office environment is completed with Student 1 only and precise indoor

localization is presented with a Student 1 only model and with a full data collection model.

In terms of the office environment, the room occupants are not aware of the data collection process while its ongoing, allowing for a data collection process that is more representative of the workday. Data collection is a continuous process until the room state is changed e.g., a room occupant stands up, changes seat location, leaves the room, etc. In that case, Student 1 who runs the data collection process, starts a new continuous data sample. Overall, Student 1 ensures the data collection process is accurate, as this student participates in each of the data collection samples. In terms of the unoccupied scenarios, Student 1 remains outside the office door, ensuring no student researcher or other university employee enters the office during this process. For the “walking” scenarios, Student 1 walked continuously in three different specified paths as included in Fig. 2. W1 refers to the first specified location for a continuous pacing path, W2 is the second, and W3 is the last. All classifications include the recorded “sitting” samples of all the students, whereas the “walking” samples of Student 1 were included for the HAR classification only.

For indoor localization, more unoccupied slots are appended to match the number of coordinates presented in a three-person example that is needed for ML. For example, a data sample of Location 1 and Location 3 would include the coordinates “(415, 70), (250, 265), (250, 10)”, as the third person is not present in the data collection process. Data for all six classifications (room classification, occupancy count estimation, relative location classification, human target differentiation, precise indoor localization, and HAR) is presented in Table 1. This table includes the number label or coordinate system used for ML, the actual label, and the number of 36 s samples for each label.

### 3.2.2 Residential Environment

Residential data collection was completed by Student 1 only for five different activities and one unoccupied scenario. As Student 1 is the only occupant for data collection, the subject knows data collection is ongoing in this case. The full complete breakdown of data collection for relative location classification, HAR, and precise indoor localization in the residential environment is included in Table 2. The five activities and their integer labels for ML are included in this table, with the addition of the coordinate system based on the activity completed. The locations are not provided the coordinate system in this case, as the activities differentiated slightly at the precise location. The unoccupied scenario was given a coordinate system close to the entrance door, like that of the office environment indoor localization. Multiple activities are completed at the same location as to prove that the system is not dependent on location for classification e.g., two activities at the same location can be differentiated based on the motion of the subject. Activity 3 of “Laying on the Ground” was included in the dataset as an activity representative of a possible fall in the geriatric population. In this instance, Student 1 remains motionless on the ground throughout the continuous data sample collection. All

activities in the dataset for the residential environment are completed continuously, where each activity is roughly 2 h of data with at most three continuous data samples for each activity.

### 3.3 Data Pre-processing

Collected data from MI-PIR was pre-processed in Jupyter Notebook using Python. To increase the data samples and allow for quicker classification times, continuous data samples were batched into 360 s samples based on the time data included in the CSV file. The 360 s time window accounts for a 36 s complete cycle at a 10 Hz sampling rate. Those that were less than 360 s samples at the end of the continuous data sample were deleted. These 360 s samples were then ready to be used in feature extraction. In total, there exists 3657 samples for the first four classifications included in Table 1, 10,971 for precise indoor localization of the full data collection model due to the splitting of individual labels and the appending of unoccupied scenarios, 1179 for precise indoor localization of Student 1, and 394 samples for the HAR classification of Student 1. For the residential environment, there are 1147 samples to be utilized for training and testing. The full complete breakdown of data collection for relative location classification, HAR, and precise indoor localization in the residential environment is included in Table 2. Data for each classification in each environment is split into 70% training, 15% testing, and 15% validation for learning purposes.

**Table 2** Data collection for the MI-PIR system in a residential environment. Locations, coordinates, and activities with their integer labels used for ML and DL are presented

Classification	Number label for ML	Real label	Available samples
Relative location classification	0	Unoccupied	185
	1	Location 1	370
	2	Location 2	208
	3	Location 3	384
Indoor localization	(425, 50)	Unoccupied	185
	(290, 260)	Working at desk	208
	(225, 150)	Laying on ground	186
	(200, 150)	Exercise on ground	184
	(125, 260)	Watch TV on bed	174
Activity recognition	(100, 270)	Sleep on bed	210
	0	Unoccupied	185
	1	Working at desk	208
	2	Laying on ground	186
	3	Exercise on ground	184
	4	Watch TV on bed	174
5	Sleep on bed	210	

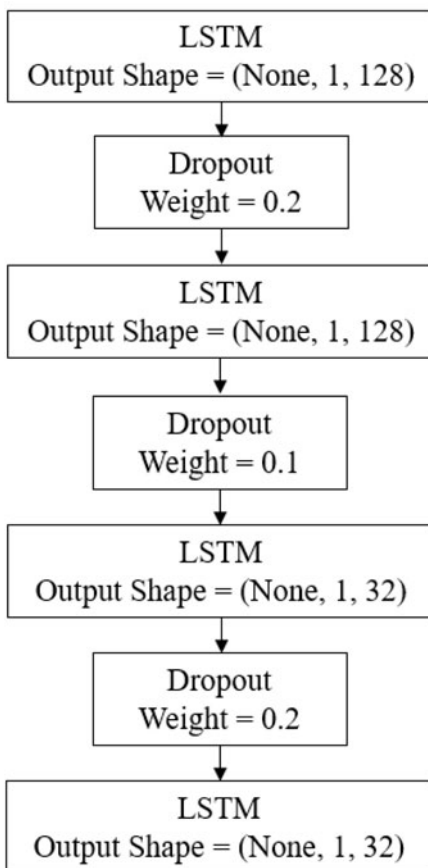
Through various feature experimentations, the signal power of the time-series raw MI-PIR analog voltage was found to be the most indicative of human presence. The signal power of the raw voltage was taken for each 360 s time window, where the absolute value of the fast Fourier transform (FFT) allowed for this calculation to be completed. This calculation was also completed with Python in the Jupyter Notebook. Other experimented features include discrete wavelet transform (DWT), raw voltage, and a standard deviation statistical feature, but all of which proved poor in stationary human presence detection using an ANN. Further, statistical testing of stationary human presence proved inadequate due to the multiple ambient environments collected over the multiple seasons in the office environment. The signal power not only achieved high accuracy for room occupancy, but for each of the other classifications. The signal power feature vector is normalized from 0 to 1 using min max normalization of the sklearn package before being used for many of the classifications. The GPR model performed better with the raw signal power, and in some cases the raw signal power showed better results in the neural networks, such as in the case of the maximum sensing distance quantification that will be presented later. Overall, the raw signal power and the normalized signal power are both used in the statistical learning models developed for the MI-PIR system.

### 3.4 AI

Four different models have been developed for MI-PIR related classifications. As mentioned, these models include three DL algorithms and one ML algorithm. An ANN, RNN, and CNN were all utilized for the four original occupancy parameters as comparison to identify the maximum accuracy obtained between the three neural networks. The GPR model is utilized for precise indoor localization. The most accurate neural network architecture will be utilized for the HAR classifications between both environments. All models in this work were built with the Keras DL framework in Python.

The ANN architectures used differ with the classification due to the number of classes outputted. For example, the human target differentiation requires eight classes, and the room occupancy classification parameter is only a binary classification which requires two classes. With that, room occupancy classification utilizes the binary crossentropy function as the loss function, and the other three parameters utilize the sparse categorical crossentropy function as the loss function. The room classification also differs in the fact that it utilizes the stochastic gradient descent (sgd) optimizer, whereas the other four classifications utilize the Adam optimizer. In general, the ANN model is composed of an input layer, a hidden layer, and output layer with multiple variations in the dimensions of each due to the number of classification output labels that are needed. For example, the ANN model for room classification of binary output consists of two dimensions for the input layer, two for the hidden layer, and one for the output layer. For an extensive table highlighting the architectures of each ANN model used for room classification, occupancy count

**Fig. 4** The RNN architecture utilized for the HAR classification in the office environment. The other RNN architectures used in this work follow a similar structure with varying output shapes due to the variation in classification



estimation, relative location classification, and human target differentiation, we direct the reader to our previous work [13].

The RNN model developed consists of two LSTM units, two dense layers, and three dropout layers to aid in overfitting of the models. The LSTM units consist of 128 dimensions, the dense layers of 32 for all but the output layer of the binary classification in which a dimension of 2 is utilized, and the dropout layers utilize 0.2 and 0.1 weights. Rectified linear unit (ReLU) and softmax are utilized for activation functions, where softmax is used as the output activation function. The Adam optimization function and sparse categorical crossentropy function are utilized for all four original models. Figure 4 presents the RNN architecture used for the HAR classification, however, the other RNN architectures used follow a similar structure. All original four occupancy classifications use 100 epochs for learning, whereas the RNN model for HAR classification uses 50 epochs.

The CNN developed includes two convolution layers, one dropout layer, one max pooling layer, and two dense layers. The convolutional layers use filters of 64 and kernel size of 3, the one dropout layers uses a weight of 0.5, max pooling layer uses a pool size of 2, and the dense layers consists of one that is 100 dimensions, and the output dense layer is the dimension of the number of labels. The relu and softmax activation functions are utilized similarly for the CNN model. Sparse categorical crossentropy is utilized for the loss function of these models and Adam is used as the optimizer function. 10 epochs are used for the CNN.

The GPR model utilized for precise indoor localization is developed with the sklearn package in Python. The MSE output of the GPR model was compared with three different kernels: Matern, RBF, and ExpSineSquared. The Matern kernel showed the best result and is thus utilized for the precise indoor localization regression problems in this work.

### ***3.5 Occupancy Parameter Classification***

The classification reports for the four original occupancy parameters using an ANN in the office environment (room occupancy, occupancy count estimation, relative location classification, and human target differentiation) were reported in our previous work [13]. The room classification occupancy parameter for detecting human presence in an office environment achieved 99% accuracy. The occupancy count estimation of differentiating between no people and, at maximum, three people achieved 91% accuracy. Relative location classification at differentiating between Location 1 through Location 5, with multiple combinations, achieved 92%. Finally, human target differentiation of eight different combinations of people with an unoccupied scenario achieved 93%.

For relative location classification in the residential environment, we used the developed RNN DL model to achieve 98% accuracy. With three locations and a constant human subject present, Student 1, the relative location classification was less complex than that in the office location. However, for an elderly monitoring system, it is imperative to know the location of the elderly individual in a non-intrusive and passive manner. The location of the elderly individual can provide peace of mind to the caregiver through the monitoring system. As such, this classification is still essential to report towards the goal of an accurate geriatric monitoring solution.

### ***3.6 Expanding MI-PIR***

Before applying the MI-PIR system to precise indoor localization and HAR, we aimed to optimize and quantify the parameters of the MI-PIR system. These metrics include the selection of an optimal DL architecture, optimal rotation time, and

maximum sensing distance. From the results, the RNN model and 36 s rotation time are found to be the optimal DL model and rotation time, respectively. From the maximum sensing distance quantification, MI-PIR can accurately detect stationary and non-stationary subjects up to 21 m. The complete results of this expansion are included below.

### 3.6.1 Optimization

In the hopes of a quicker classification time, the optimal rotation time for classification of the room occupancy parameters in the office environment was experimented with. Three different classification times were addressed for comparison. These include 36 s for a complete rotation of the robotic actuator, 26 s for the front scan only, and 10 s for the backward scan only. This analysis was completed within the developed Python code, where the batches were first developed for the 36 s rotation time. Following, the last 10 s would be removed for the 26 s examination and vice versa for the 26 s classification. Thirty-six seconds proved to be the most accurate of the three times, and despite the additional time required, the relatively large increase in accuracy outweighs the additional classification time. The results of this optimization are included in Table 3 with reported accuracies from the previously developed ANN.

The RNN and CNN introduced in this section were developed to compare the reported accuracies from the ANN to more sophisticated models. The results of this optimization are also presented in Table 3 for each of the four occupancy parameters in the office environment. From these results, the RNN is shown to be the most accurate DL model for MI-PIR, as indicated by the maximum accuracy obtained for each of the occupancy classifications. The RNN performing the best in these four classifications is expected due to the time-series nature of the input data. The RNN model will be utilized for the rest of the work due to these results.

### 3.6.2 Quantification

Utilizing the RNN DL model, we aimed to quantify the maximum sensing distance for possible extension of the design to larger environments. In addition, this metric would allow for better comparison to existing human monitoring systems. In this experiment, we collected data of Student 1 walking and standing at iterative linear distances away from the MI-PIR system in three different ambient environments: a residential hallway, a construction warehouse, and a gymnasium. Three ambient environments were included as there was a need for greater distance away from the sensor following the results of each environment. In the residential environment, data was collected for an unoccupied scenario and from 1 to 12 m away from the MI-PIR system. In the construction warehouse, data was collected for an unoccupied scenario and 13 through 19 m away from MI-PIR at 1 m increments. In the gymnasium, data was collected for an unoccupied scenario and distances at

**Table 3** The results of the optimization of metrics used in the original MI-PIR system. The DL model and rotation time are optimized to advance the novel system

Optimization metric						
DL	Model	Room classification (%)	Occupancy count (%)	Location classification (%)	Human target differentiation (%)	
	ANN	99	91	93	93	93
	RNN	100	93	95	94	94
	CNN	100	90	93	94	94
Rotation time	Time(s)	Room classification (%)	Occupancy count (%)	Location classification (%)	Human target differentiation (%)	
	36	99	91	93	93	93
	26	98	84	84	89	89
	10	75	71	69	80	80

21, 41, and 43 m. For walking data collection in these environments, the human subject paced a few meters back and forth, whereas for stationary data collection, the human subject remained seated during the entirety of the collection. The maximum sensing distance for a stationary individual and moving individual was quantified by removing the data sample with the next farthest distance to quantify the RNN accuracy. The manufacturer lists the maximum sensing distance of the Panasonic AMN24112 PIR sensor as 10 m with the deployment of a PIR sensor in the traditional approach. The results of this maximum sensing quantification are compared between three different sample sets, one in which all the data is included, one of just motionless data, and one of just walking data. The results of this quantification are included in Table 4.

For each occupied scenario, about 3–5 min of data was collected with matching unoccupied scenarios at each ambient environment for balanced data. Therefore, in total, there exists 426 samples for maximum sensing distance quantification. With motion and motionless data combined, the maximum sensing distance for 100% accuracy was quantified as 41 m. With motionless data only, maximum sensing distance for 100% accuracy was found to be 21 m. Finally, for motion data only, the maximum sensing distance was also reported as 21 m.

From these reported results it is evident that MI-PIR has human detection capabilities beyond the reported 10 m distance reported by the manufacturer. The maximum sensing distance is quantified between three ambient environments, causing the DL model to learn from multiple locations. For more accurate maximum sensing quantification, data should be collected at one central location. The data collection and results of this work is more robust however, due to the multiple ambient environments. With the large jump between 21 to 41 m at the gymnasium location, the maximum sensing distance could be greater than the reported 21 m for stationary and non-stationary human subject detection. The 41 m maximum sensing distance quantification, which includes all the data, allows for learning of double the number of scenarios. With the additional training data, the distance of the monitored human subject is expanded. Verification of the maximum sensing distance will be addressed with additional data at the gymnasium location. With that being said, the MI-PIR system has shown to expand the sensing distance of the traditional analog PIR sensor to a recorded 21 m with motion and motionless data only, and even further with all the data included.

### ***3.7 Precise Indoor Localization via GPR***

The GPR model was applied for a regression method of indoor localization. The regression method, in comparison to the relative location classification, allows for estimation of the human occupant in comparison to the ground truth coordinate system. The coordinate system utilized for the precise indoor localization in the office environment is presented in Table 1. Two classifications are completed for the precise indoor localization in the office environment: one in which all stationary

**Table 4** MI-PIR maximum sensing distance quantification of three different ambient environments using an RNN DL model. One subject sits and paces at iterative distances away from the sensor system for 3–5 min of continuous samples. The results present below indicate human detection sensing distance classification of including the farthest distance in the RNN DL model

Ambient environment	Environment type	Max. measured length (m)	Distance (m)	All data: Accuracy (%)	Motionless: Accuracy (%)	Motion: Accuracy (%)
Residential hallway	Rectangular hallway	12	1	100	100	100
			3	100	100	100
			7	100	100	100
			9	100	100	100
			10	100	100	100
			11	100	100	100
			12	100	100	100
			13	100	100	100
			14	100	100	100
			15	100	100	100
			16	100	100	100
			17	100	100	100
Construction warehouse	Square facility	19	18	100	100	100
			19	100	100	100
			21	100	100	100
			41	100	95	98
			43	95	91	95
			47			
Gymnasium	Square gymnasium	47	21	100	100	100
			41	100	95	98

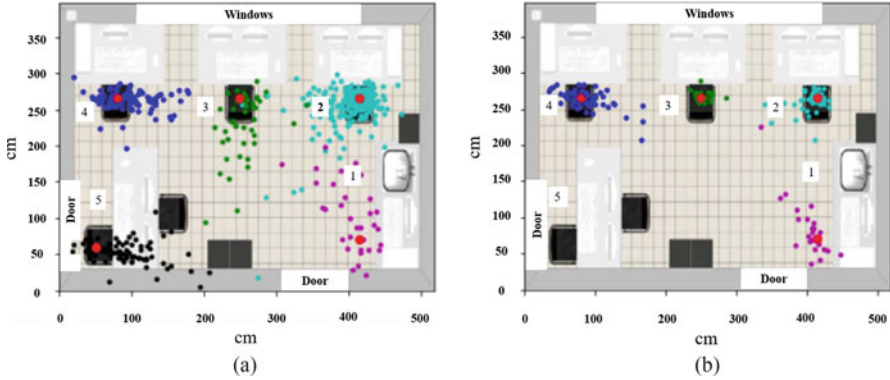


**Fig. 5** Result of precise indoor localization using GPR with (a) all data (unoccupied result not shown) and (b) Subject A

data collected is utilized and another in which only the data from Student 1 is utilized. The Student 1 only model does not include data from Location 5 or any unoccupied data, whereas the model including all the data does include the unoccupied scenarios. Including two different regressions allows for a comparison of the models in learning from the signal power from multiple subjects in the office space to one in which there is only one person accounted for.

For multiple people, the MSE obtained is  $493.7 \text{ cm}^2$ . The accuracy of this model may be better represented visually. Figure 5(a) presents the accuracy of the model for precise indoor localization using a GPR model with a Matern kernel and with all the data collected for multiple variations in students present in the office environment. This model does not visually include the clustering of the unoccupied scenario, which is located near the door, as this data was only included as a means of balancing the data to match the coordinate systems of three people. With all the ground truth data for each location presented as red dots, and the estimations presented in varying colors, one can determine that the developed GPR model proved sufficient at clustering the testing data in their respective locations. With the Student 1 only model, on the other hand, the model produced a MSE of  $426.4 \text{ cm}^2$ . Although a better resulting MSE than the model with multiple people, the MSE is relatively similar. Also, based on the visual representation in Fig. 5(b), the clusters for the four respective locations of Student 1 are developed. The results of this work indicate that MI-PIR proves to not only classify locations in an office environment, but also estimate these locations in terms of coordinate systems. The exact coordinates of the students were not measured during training data and the student researchers were also free to subtly move their chairs. As a result, the MSE is not an exact indicator of the performance of these models, but rather this exercise proves to be a sufficient method for clustering of testing coordinates to the ground truth coordinate system. With more precise ground truth data, the MSE is hypothesized to decrease for both the full data collection method and for Student 1 only.

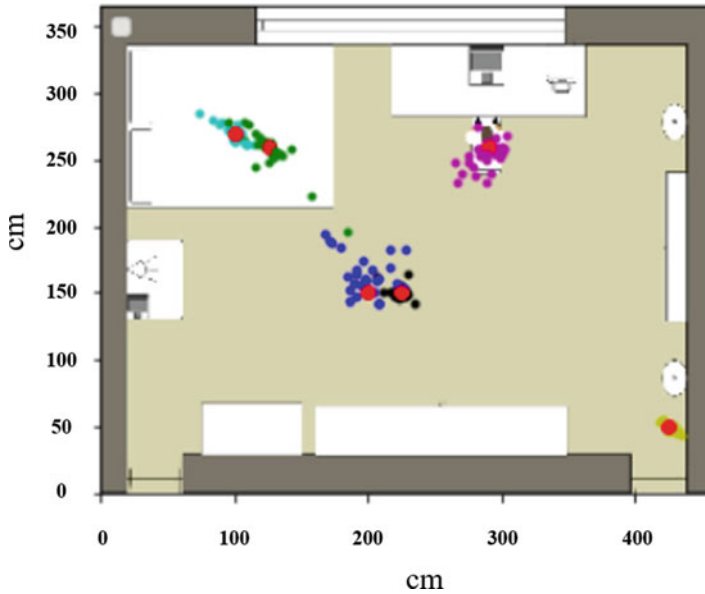


**Fig. 6** GPR model of the residential environment, where each color represents a different activity. The yellow cluster near the entrance represents the unoccupied scenario

For precise indoor localization with a GPR model in the residential environment, the reported MSE is  $131.4 \text{ cm}^2$ . For better understanding of this reported metric, the modeled residential environment provides the clustering of the precise locations of each activity, as shown in Fig. 6. This model also proves accurate at clustering the locations of the activities. As a comparison, the GPR model can be more accurate in indoor localization as the estimation of future activities can be applied throughout the environment, whereas the classification of locations is either classified correctly or not. The unoccupied scenario is included in this visual display of the model, as indicated by the small yellow cluster close to the entrance door in Fig. 6.

### 3.8 HAR

As a proof of concept, a simple HAR classification model was developed for the office environment. Simple classification of sitting, walking, and an unoccupied scenario was hypothesized to show some level of indication that MI-PIR could accurately classify various activities in its FoV. The results of this classification would allow for expansion to a residential environment for a HAR system more indicative of the activities that an elderly individual would complete.

Student 1 data was only utilized in this classification. This data included stationary moments from the original data collection that was utilized in prior

classification and regression problems. Specifically, this stationary data included samples from Location 2 and Location 4. In addition, this dataset includes walking sets from all the walking patterns: W1, W2, W3. In these instances, Student 1 paced for as long as 15 min, providing continuous data samples of walking data to classify. Overall, there exists 394 samples to be utilized for classification as presented in Table 1. With the 70%, 15%, 15% split of training, testing, and validation data that is completed in all the models referenced in this work, there exists 275 samples for training and 59 samples for testing.

The RNN model was utilized in this case for HAR classification in an office environment. The model proved 100% accurate at differentiating unoccupied, sitting, and walking scenarios completed by Student 1. The RNN proved its superiority with time-series data such as in the case of the normalized absolute value of the FFT. These results indicate that the MI-PIR system could prove accurate as a HAR system in a geriatric monitoring situation. To prove this hypothesis, MI-PIR was utilized in a residential environment for classification of additional activities.

Based on the success of the HAR classification in the office environment and towards the development of an elderly monitoring system, accurate HAR classification in a residential environment is an important task. With early success from differentiating walking from sitting in the office environment, this classification aims to extend the number of activities classified in a residential environment. The developed RNN model achieved 98% accuracy in this classification of five different activities and an unoccupied scenario. Two activities, “Exercising on Ground” and “Laying on Ground”, were completed at Location 1, and two other activities, “Watching TV on Bed” and “Sleeping on Bed”, were completed at Location 3. The model proves robust to differentiating activities at the same location, indicating that the variations in infrared radiation as indicated by the absolute value of the FFT are suitable for an accurate HAR model in a residential environment. The classification of the “Laying on Ground” label indicates the efficacy of detecting a potential fall event and classifying such activity in 36 s increments. This also would allow for greater state of mind of the caregiver in terms of an accurate elderly monitoring system. The accuracy of the RNN model utilized for this HAR classification is presented visually as a confusion matrix in Fig. 7. The integer labels provided on the confusion matrix correlate to the activities highlighted in Table 2. From this confusion matrix, one can identify high classification results, with only minimal confusion relating to the activity number label of “3” or real label of “Exercise on Ground”.

## 4 Chest Motion PIR

MI-PIR was developed as a novel system for stationary human detection utilizing only one analog PIR sensor. Similarly, a system relying on the detection of the chest motion of a perfectly still stationary human subject for stationary human presence detection using one analog PIR sensor has been developed. This system is coined

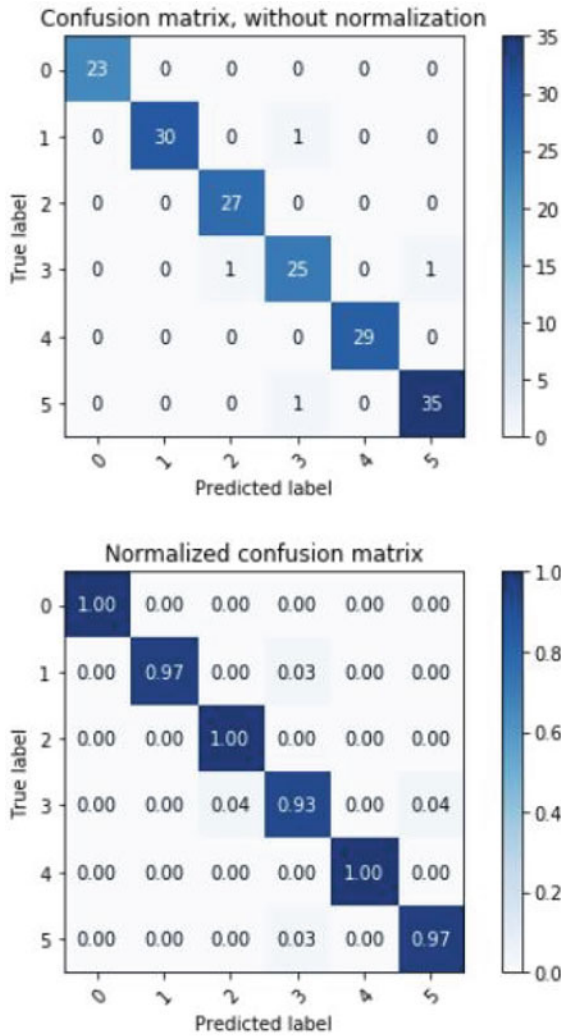


**Fig. 7** Confusion matrix for HAR in the residential environment. The accuracy of HAR is reported as 98%, and the confusion matrix serves to highlight this reported accuracy. True labels and predicted labels are provided with integer labels that correspond to the activities provided in Table 2 for HAR in a residential environment

CM-PIR and has been previously presented in our past work [14]. CM-PIR consists of the Panasonic AMN24112 PIR sensor, an Elegoo Uno R3 microcontroller, a PC, and the RNN DL model for human detection and biometric authentication classification.

CM-PIR is based on the resting heart rate estimation using a PIR sensor methodology from related work, where the users are perfectly still 1 m away

during the data collection process [65]. The filter to extract the heart rate from the individuals was presented in the introduction of this work in Eq. (3). Our first step in the human detection and biometric authentication process using CM-PIR was to verify the accuracy of the filter and estimating the human heart rate of individuals using a PIR sensor. After verifying this work with the heart rate monitor of the Apple Watch Series 3, we expanded the data collection process to include 16 subjects at nine different ambient environments. The accuracy of the model achieved 94% for human detection and 75% for biometric authentication of Subject A against all other potential adversaries. The results of this work are aimed to be utilized in a desk scenario, where the human subject can be detected and authenticated for security purposes at a 1-m distance.

## ***4.1 Data Acquisition***

CM-PIR successfully collected data for 16 subjects at nine different ambient locations. Each subject recorded data for at least 20 min, with many collecting for more trials and at various ambient environments. The subjects are of varying ages and sex, with the ages of the subjects ranging from 15 to 60 years old and six females and ten males included in the study. Some of the subjects utilized for the CM-PIR data collection are of family relation. In each ambient environment, the CM-PIR system would be set-up 1 m away on a surface that was on the chest level of the subject. The full data collection for the CM-PIR system is presented in Table 5.

## ***4.2 Data Pre-processing***

Upon data acquisition of 16 subjects at nine different locations, the data was pre-processed in Python. The overall CM-PIR flowchart is included in Fig. 8. In a similar manner to how the MI-PIR data was batched according to the rotation time, the CM-PIR data was batched to increase the number of data samples from the original data files. This involved identifying the optimal window size experimentally. The optimal window size was determined to be 90 s based on a balance between the number of available samples to learn from and the number of data points to be learned from. With the 90 s optimal selection in place, the next process was to apply a threshold to the raw PIR voltage data. In terms of a human subject in motion, the raw analog PIR voltage will spike from 5 V to 0 V as indicated by a sinusoidal swing. In terms of the early data collection of CM-PIR, the motion of the chest from a perfectly stationary human subject is between the ranges of 3 V to 2 V. To account for different ambient environments, a threshold of 3.5 V to 1.5 V was applied to the 90 s batches. If there are any data points greater than 3.5 V or less than 1.5 V in the sample, that 90 s batch would be removed. As a result, Table 5 indicates the available samples from the collected samples after the threshold was applied. With the threshold, four

**Table 5** Data collection for the CM-PIR system including the data distribution for stationary detection, biometric authentication, and overall subject distribution. The data included is for a 90 s window size and 3.5 to 1.5 V threshold that reduced the number of available samples from collected to used

Category	Data collected (samples)	Data used (samples)	Integer label	Real label	Location
Stationary detection	123	122	0	Unoccupied	A-D
	443	295	1	Occupied	A-I
Biometric authentication	123	122	0	Unoccupied	A-D
	219	133	1	Subject A	A-D
	224	162	2	Adversaries	B, D-I
Individual subject distribution	123	122	0	Unoccupied	A-D
	219	133	1	Subject A	A-D
	40	34	2	Subject B	A-C
	19	19	3	Subject C	B
	35	32	4	Subject D	B
	18	14	5	Subject E	E
	9	7	6	Subject F	E
	11	11	7	Subject G	B
	6	0	8	Subject H	F
	14	0	9	Subject I	G
	13	11	10	Subject J	G
	12	6	11	Subject K	B
	7	0	12	Subject L	H
	12	0	13	Subject M	I
	13	11	14	Subject N	F
	12	7	15	Subject O	F
13	10	16	Subject P	D	

human subjects and three ambient environments were completely removed from the dataset. As a result, CM-PIR would then detect and classify 12 subjects and an unoccupied scenario from six different ambient environments.

Following both the window size selection and applied threshold, feature calculations were then made on this data. As indicated by the MI-PIR system, the absolute value of the FFT proved to be an accurate feature for human presence and related occupancy parameters. This feature was used for the CM-PIR data, as a result. Indicated in orange in Fig. 8, three additional steps in the CM-PIR flowchart are included for the biometric authentication classification only. With that, two more feature calculations are made on the CM-PIR data for concatenation to be utilized in the biometric authentication classification of Subject A against all other adversaries.

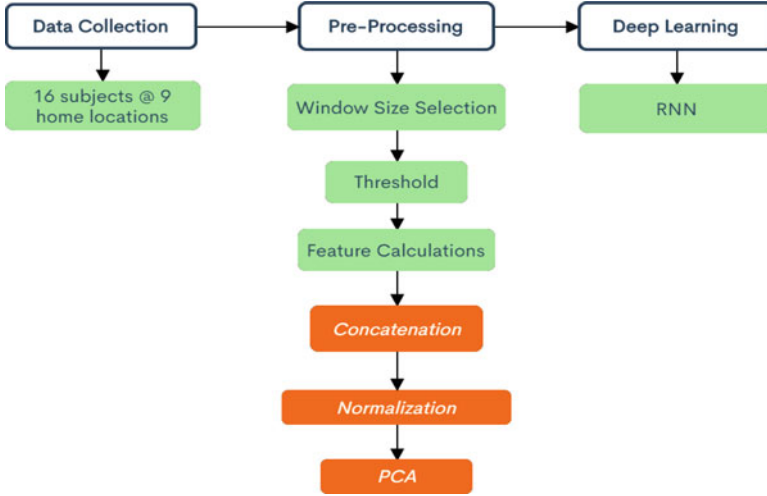


**Fig. 8** CM-PIR flow chart. The orange is for biometric authentication only and the green is for both human detection and biometric authentication classifications

The first additional feature to be used for biometric authentication is the acceleration filter that models the response of the heart from the chest motion movement. The absolute value of this feature is computed and concatenated to the signal power value. The last feature to be utilized for the biometric authentication classification is the absolute value of the DWT. The DWT feature allows for the frequency and time in location of the raw PIR data to be represented in one feature and has been utilized in related work for biometric authentication. Thus, the absolute value of the FFT, acceleration filter, and DWT are concatenated for biometric authentication in this work.

For the concatenated feature set to be of relative magnitude, we applied the sklearn min max normalization to map the values from zero to one. Following this normalization, PCA was then applied to reduce the dimensionality of the feature set from 2700 data points to five data points. Not only does PCA reduce the dimensionality of the normalized, concatenated feature set, but it also works to identify the values that are representative of the entire vector. As such, PCA increased the accuracy of the biometric authentication classification. Once PCA was applied, the 900-sample human detection feature set and the feature set of five for biometric authentication could be applied to the RNN DL model.

### 4.3 Recurrent Neural Network (RNN)

To learn the complex feature set originating from the chest motion data captured by one analog PIR sensor, a DL model is proposed. In that case, a similar RNN model

to that of the MI-PIR classifications is developed. A similar RNN is proposed in this case due to the success that the RNN shown in classifying time-series data from the MI-PIR system. Towards this, the RNN consists of two LSTM layers, three dropout layers, and two dense layers. The LSTM layers are composed of 128 dimensions and the dense layers are composed of 16 dimensions. The dropout layers have a weight of 0.1 to aid in overfitting, which was initially a problem with a relatively limited dataset for biometric authentication. All the layers of the RNN model utilize the ReLu activation function except for the last dense layer which utilizes the softmax activation function. In terms of the loss function and optimizer utilized in this model, the sparse categorical crossentropy loss function and Adam optimizer are again utilized. Both classifications underwent 125 epochs. We direct the reader to our previous work for a visual representation of the RNN architecture used with CM-PIR [14] The results of these classifications will be presented in the subsequent sub-sections.

#### ***4.4 Human Detection***

The human detection classification achieved 94% accuracy after training on 291 samples and testing on 63 samples as a resultant of a 70% training, 15% testing, 15% validation split. In comparison to the MI-PIR system, CM-PIR achieved lower detection accuracy using one analog PIR sensor; however, the CM-PIR system requires less additional architecture. Utilizing only the analog PIR sensor and the microcontroller for data transmission, the set-up time and cost is much lower with CM-PIR. In comparison to other proposed models for stationary human presence detection using one PIR sensor, the CM-PIR system utilizes less additional hardware. As a standalone PIR sensor that relies on software processing and statistical learning for accurate classification, the novel CM-PIR system advances the capabilities of PIR sensor human monitoring. Based on the chest motion data at a 1-m distance, the CM-PIR system would accurately respond to a desk situation in which the human subject was completely motionless.

#### ***4.5 Biometric Authentication***

The biometric authentication system based on the chest motion data captured by a PIR sensor achieved an accuracy of 75%. These initial results prove the potential efficacy of using a PIR sensor for security purposes. With pre-processed data collection of 12 individuals at six different home locations, the PIR sensor had to differentiate the many ambient environments from the human subjects, as well as authenticate the users based on their unique chest motion movement. With less ambient environments collected for in the data collection process, we hypothesize that these initial results would increase, as with related non-contact

biometric authentication systems, data collection occurred at only one central location. In terms of PIR sensors, multiple testing locations causes even more ambient interference in recording of chest motion data. The CM-PIR recorded accuracy, however, is much more robust as a biometric authentication system due to the many ambient environments. As with many systems that rely on DL for classification, we hypothesize that increased data collection of the subjects involved in the study would increase the accuracy of the results. Due to the balancing of an optimal window size selection in terms of data points and data samples, there are limited 90 s batches to learn from. Increasing the data collection efforts could improve the results, especially in the cases of those subjects that were completely removed from the study due to the applied threshold.

## 4.6 Quantification

New in this work is the addition of the quantification of the maximum sensing distance of the CM-PIR system for accurate detection of stationary human subjects. As the original data collection was present at a 1-m distance, we extend the CM-PIR system for possible detection at a 2 m and 3 m distance. In this quantification, data was collected by Subject A at Location D for 30 min at 1 m, 2 m, and 3 m, with an additional equal time length of unoccupied data collection. In a similar methodology of removing the dataset of longest distance iteratively from the DL model, 3 m was classified with 85% accuracy and 2 m was classified with 92% accuracy. At 1 m, with one ambient environment and one subject, the CM-PIR system detected human subjects with 96% accuracy. With these results in mind, a 1-m distance is proven to be the maximum sensing distance for an accurate stationary human detection system.

## 5 Discussion

PIR sensors are discussed as potential long-term monitoring solutions due to their low cost, non-contact, non-intrusive, and relatively accurate and reliable results. In terms of cost, the Panasonic AMN 24112 PIR sensor used in both systems proposed in this work costs roughly \$30 USD, whereas the Microsoft Kinect sensor used in video-based solutions costs roughly \$75 USD. This comparison in cost can be illuminated further when systems rely on multiple video-based modalities for accurate detection, and whereas the proposed solutions in this work require only one sensor modality [54]. Furthermore, the Impinj RAIN RFID reader that is used in related work can cost upwards of \$1000 USD [38]. From this, one can identify that the proposed PIR sensor-based systems for human detection and biometric authentication are relatively inexpensive in comparison to systems proposed in related work due to their reliance on only a single COTS sensor modality. With

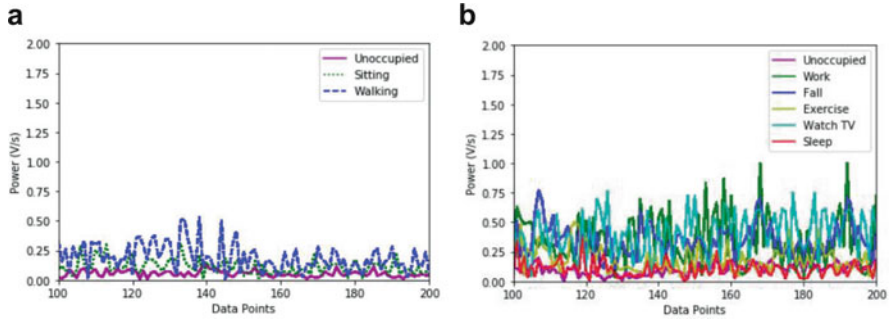


**Fig. 9** FFT plot of HAR in (a) an office environment and (b) a residential environment indicating the differences seen between activities

that, the non-contact, non-intrusive, and accurate nature of PIR sensors makes them suitable modalities for long-term monitoring systems.

The major known drawback with PIR sensors is their inability to detect stationary human subjects reliably and accurately in their FoV. In this work we have introduced two novel systems to combat this major known issue with PIR sensors. MI-PIR is a motion induced PIR sensor system that classifies an office space for room occupancy, occupancy count, relative and precise location, human target differentiation, and simple HAR every 36 s of rotation time. In a residential environment, MI-PIR classified relative and precise locations of one individual subject, as well as showed the efficacy of a more complex HAR classification. CM-PIR on the other hand deploys one PIR sensor in the traditional sense for accurate human detection and biometric authentication for security of IoT devices.

The signal power, or the absolute value of the computed FFT coefficients from the raw PIR voltage data, proved to be a strong feature for the detection of stationary human subjects using an analog PIR sensor. To alleviate the black-box stigma that surrounds DL classification models, we present Fig. 9 which identifies one 36 s batch of each activity collected for during the MI-PIR office and residential data collection. Figure 9(a) indicates the varying signal power for each activity completed in the office environment and Fig. 9(b) indicates the varying signal power for each activity completed in the residential environment. The office environment presents the walking situation to have a greater signal power than the sitting situation, with the unoccupied scenario showing significantly lower signal power. The residential environment signal power comparison presents varying signals that align with our hypotheses. During a work scenario in which the user is seated, working, and using electronics, there would be higher levels of signal power than during the sleep and unoccupied data collections. In a direct comparison of two activities at the same location, “Watching TV on Bed” and “Sleeping on Bed”, the latter activity had much less signal power due to both the lack of electronics in use, as well as the lack of movement while sleeping.

**Table 6** Comparison of novel systems for stationary human presence detection using one PIR sensor. The models are compared for their solution, methods, FoV, maximum sensing distance, and stationary human presence detection accuracy

Classification	Reference	Proposed solution	Methods	Horizontal FoV (°)	Max. sensing (m)	Accuracy (%)
Stationary human presence	Juan et al. [18]	Optical shutter	Presence—Voltage	110	7	100
	Wu and Wang [22]	Optical shutter	Presence—Voltage	93	4.5	100
	MI-PIR	Motion induced	Classification—RNN	223	19	100
	CM-PIR	Chest motion	Presence—RNN	93	1	94

For comparison of these proposed systems to systems of related work, we highlight Table 6 which includes this information. MI-PIR, CM-PIR, and related work on using a PIR sensor for stationary human presence detection is compared in this Table. MI-PIR through rotation of the analog PIR sensor extends the manufacturer reported horizontal FoV from 93 to 223° through a 130° rotation. In addition, based off the maximum sensing distance quantification, the maximum sensing distance of a stationary human subject was found to be 21 m. For CM-PIR, these results are the manufacturer stated 93° through the deployment in a traditional sense and a 1 m maximum sensing distance. In comparison to related work, MI-PIR extends the FoV for monitoring and extends the maximum sensing distance. For CM-PIR, the FoV, maximum sensing distance, and accuracy is reduced. CM-PIR is however the only solution that requires no additional hardware. As MI-PIR is less mechanically complex than the other systems in related work that require the development of an optical shutter for the analog PIR sensor, CM-PIR requires no robotic actuator for accurate stationary human presence detection.

In terms of differentiating the results of the MI-PIR system with related work in HAR classification, the MI-PIR proves superior as presented in Table 7. MI-PIR produces a higher accuracy of differentiating unoccupied, sitting, and walking activities than in related work. From a 100% accuracy to a 93% accuracy, one can determine that the MI-PIR system is more accurate as a simple HAR classification. Although classification in the related work is through a continuous data collection with multiple people, the accuracy of the MI-PIR system with multiple activities in a residential environment ensures the potential superior efficacy to the related work [22]. The MI-PIR system for classification of a residential environment is compared to the results of the *ALPAS* system presented earlier. This system requires two PIR sensors for HAR classification, whereas the MI-PIR system requires only one analog PIR sensor. The accuracy of the MI-PIR system of classifying five activities with one unoccupied scenario achieves a significantly higher accuracy than the reported F-measure of the *ALPAS* system. Although the *ALPAS* system classifies four activities at one location with multiple users participating in the study, the MI-PIR system's significant increase in accuracy ensures the superior efficacy to the *ALPAS* system [48].

For comparison of CM-PIR with other biometric authentication systems, CM-PIR classifies one human subject against 11 other individuals that remain in the study following an applied threshold. The 75% accuracy of CM-PIR is compared against the introduced *Cardiac Scan* system of 98.6% accuracy with 78 different subjects. Although the *Cardiac Scan* system achieves much greater accuracy, there are a variety of differences between the two systems that highlights the potential positives that CM-PIR might provide. CM-PIR collects data from nine different ambient environments, although three of which are removed with a threshold during pre-processing. In contrast, *Cardiac Scan* collects data at one central location. The multiple ambient environments that the CM-PIR system must learn from is hypothesized to decrease the accuracy and will be tested in future work. The PIR sensor in which CM-PIR relies on is a passive sensor, and *Cardiac Scan* utilizes an

**Table 7** HAR and biometric authentication classification accuracy comparison against similar proposed systems in literature

Classification	Reference	# of PIRs	# of activities	Activities	Results
HAR—Office	Wu and Wang [22]	1	3	<ul style="list-style-type: none"> <li>- Unoccupied</li> <li>- Sitting</li> <li>- Walking</li> </ul>	93% accuracy
	MI-PIR	1	3	<ul style="list-style-type: none"> <li>- Unoccupied</li> <li>- Sitting</li> <li>- Walking</li> </ul>	100% accuracy
HAR—Residential	Kashimoto et al. [48]	2	4	<ul style="list-style-type: none"> <li>- Eat on sofa</li> <li>- Read of sofa</li> <li>- Use phone on sofa</li> <li>- Use PC on sofa</li> </ul>	57% F-measure
	MI-PIR	1	6	<ul style="list-style-type: none"> <li>- Unoccupied</li> <li>- Working at desk</li> <li>- Laying on ground</li> <li>- Exercise on ground</li> <li>- Watch TV on bed</li> <li>- Sleep on bed</li> </ul>	98% accuracy

active Doppler Scanner for biometric authentication [66]. The passive nature of the sensor would allow for greater state-of-mind with less chance of any adverse health and energy concerns.

## 6 Conclusions

Elderly monitoring remains an ever-growing challenge due to the increasing number of individuals and the prevalence of neurodegenerative diseases found in this population. Current systems for monitoring aging subjects often rely on camera-based or terminal-based modalities that cause both a privacy intrusion and burden to the end-user. Ambient sensors have been proposed to fill the gaps towards a need for non-contact and non-intrusive monitoring systems that provide both accurate localization and HAR classification of aging individuals in a residential environment. Many of these current systems require expensive architecture or multiple sensors deployed throughout the room to expand the FoV. Towards the goal of accurate localization, HAR, and other occupancy related parameters, a novel system coined MI-PIR was proposed in this work. CM-PIR is proposed in this work for human detection and biometric authentication. To summarize the contributions of these two systems, the accuracies and quantifications are included below.

In summary, MI-PIR has shown these results in an office environment utilizing statistical learning . . .

- 100% accurate at room classification,
- 93% accurate at occupancy count estimation,
- 95% accurate at relative location classification,
- 94% accurate at human target differentiation,
- 100% accurate at simple HAR,
- 493.7 cm<sup>2</sup> MSE was quantified for precise indoor localization with varying subject conditions,
- 426.4 cm<sup>2</sup> MSE was quantified for precise indoor localization of Subject 1 only.

MI-PIR has also shown accurate results in a residential environment utilizing statistical learning . . .

- 98% accuracy at relative location classification,
- 98% accurate at differentiating five activities and an unoccupied scenario.
- 131.4 cm<sup>2</sup> was quantified for precise indoor localization of Subject 1 only.

CM-PIR has shown to be accurate in two different classifications . . .

- 94% accurate at human detection of perfectly stationary human subjects,
- 75% accurate at biometric authentication of 13 labels at six varying environments.

These results highlight the potential success of MI-PIR as a long-term elderly monitoring solution and CM-PIR as both a monitoring solution and biometric authentication modality. In the case of HAR for MI-PIR, similar results to those reported above can be obtained via the monitoring of one elderly subject, whereas

additional tests are required to determine the efficacy of HAR with many individuals present in an indoor environment. For each other classification, multiple subjects were included, and the results can be directly mapped to a real-world scenario. The only requirement for deployment of MI-PIR would be to collect initial training data of the ambient environment.

While MI-PIR is proposed as a potential elderly monitoring system, CM-PIR is proposed as a combined office space occupancy detection and IoT security system. The FoV of the CM-PIR system is constrained to the manufacturer stated FoV, as this analog PIR sensor is deployed in the traditional sense. As such, CM-PIR is proposed to be deployed at the desk location of a human subject present in an office scenario. Accurate detection of a human subject, even in the most motionless of instances, would aid in smart energy management applications in an office environment. The novelty of the CM-PIR system for stationary human presence detection against proposed methods, including MI-PIR, is the lack of additional hardware and set-up needed. In comparison to a state-of-the-art non-contact biometric authentication system, CM-PIR proves less accurate, but proposes a more adequate sensor modality for long-term monitoring. Data collection at one central location, as well as a greater data collection effort, is hypothesized to increase the initial results of CM-PIR for biometric authentication. CM-PIR would be suitable for human detection in a real-world office environment, but only suitable as a biometric authenticator in a closed room with a single individual. The CM-PIR biometric authentication system extends the capabilities of biometric authentication systems from traditional contact systems to an additional non-contact system. Non-contact and non-intrusive biometric authentication systems for IoT security is a growing need with the ever-growing field of IoT devices in our everyday life.

The summarized results also indicate the efficacy of the RNN model at classifying various scenarios. The RNN proved the most accurate DL model, indicating the temporal reliance of the signal power feature calculated in data pre-processing. With precise indoor localization using a GPR model, MI-PIR showed to be effective at visually clustering locations in two ambient environments, allowing for regression of future coordinate systems during real-world deployment of the system. These activities differentiated in the residential environment proved the potential success as an elderly monitoring modality. In fact, classifying a “Laying on Ground” activity proved direct translation to a potential fall event. Accurately classifying multiple activities that are performed at the same location proves the HAR classification accuracy is not based on the learning of the location in which the activity is performed.

The future of monitoring is in the deployment of ambient sensors with statistical learning algorithms for accurate localization and HAR classification. To fulfill the needs of a non-contact, non-intrusive, low-cost, and passive sensor modality for monitoring situations, a PIR sensor is proposed and highlighted in this work. Solving the known drawback of PIR sensors in this work with two novel systems, the capabilities of PIR sensors for monitoring have been extended. Future work for progression of these two novel systems include testing the MI-PIR system for a real-world data collection and increasing the biometric authentication accuracy of the CM-PIR system. A more systematic data collection and increased data collection is

proposed to increase the biometric authentication accuracy of the CM-PIR system. These novel systems highlight the growing field of ambient sensing for human detection and biometric authentication.

**Acknowledgments** This research is supported by AFOSR grant FA9550-18-1-0287.

## References

1. United Nations, D. of E. and S. A. P. D. (2020). *World population ageing 2019* (ST/ESA/SER.A/444). Retrieved from [https://www.un.org/development/desa/pd/sites/www.un.org.development.desa.pd/files/files/documents/2020/Jan/un\\_2019\\_worldpopulationageing\\_report.pdf](https://www.un.org/development/desa/pd/sites/www.un.org.development.desa.pd/files/files/documents/2020/Jan/un_2019_worldpopulationageing_report.pdf).
2. Milken Institute School of Public Health at The George Washington University. (2018, April 6). *The growing cost of aging in America Part 1: An aging population and rising health care costs*. Retrieved from <https://onlinepublichealth.gwu.edu/resources/cost-of-aging-healthcare/>.
3. Vespa, J., Armstrong, D. M., & Medina, L. (2020, February). *Demographic turning points for the United States: Population projections for 2020 to 2060*. United States Census Bureau. Retrieved from <https://www.census.gov/library/publications/2020/demo/p25-1144.html>.
4. de Nardi, M., French, E., Jones, J. B., & McCauley, J. (2015, June). *Medical spending of the elderly*. National Bureau of Economic Research. Retrieved from <https://www.nber.org/bah/2015no2/medical-spending-elderly#:~:text=Medical%20spending%20by%20the%20elderly,percent%20of%20all%20medical%20spending>.
5. Gitler, A. D., Dhillon, P., & Shorter, J. (2017). Neurodegenerative disease: Models, mechanisms, and a new hope. *Disease Models & Mechanisms*, 10(5). <https://doi.org/10.1242/dmm.030205>.
6. Gómez-Gómez, M. E., & Zapico, S. C. (2019). Frailty, cognitive decline, neurodegenerative diseases and nutrition interventions. *International Journal of Molecular Sciences*, 20(11). <https://doi.org/10.3390/ijms20112842>.
7. Agrawal, M., & Biswas, A. (2015). Molecular diagnostics of neurodegenerative disorders. *Frontiers in Molecular Biosciences*, 2. <https://doi.org/10.3389/fmolb.2015.00054>.
8. Obaidat, M. S., Rana, S. P., Maitra, T., Giri, D., & Dutta, S. (2019). Biometric security and internet of things (IoT). In M. S. Obaidat, I. Traore, & I. Woungang (Eds.), *Biometric-based physical and cybersecurity systems* (pp. 477–509). Springer International Publishing. [https://doi.org/10.1007/978-3-319-98734-7\\_19](https://doi.org/10.1007/978-3-319-98734-7_19)
9. Alraja, M. N., Farooque, M. M. J., & Khashab, B. (2019). The effect of security, privacy, familiarity, and trust on users' attitudes toward the use of the IOT-based healthcare: The mediation role of risk perception. *IEEE Access*, 7. <https://doi.org/10.1109/ACCESS.2019.2904006>.
10. Adjabi, I., Ouahabi, A., Benzaoui, A., & Taleb-Ahmed, A. (2020). Past, present, and future of face recognition: A review. *Electronics*, 9(8). doi:<https://doi.org/10.3390/electronics9081188>.
11. Adra, B. (2019). Facing the facts on biometric phone locks: Your face and thumb are not secure.
12. Yang, W., Hu, J., Wang, S., & Wu, Q. (2018). Biometrics based privacy-preserving authentication and mobile template protection. *Wireless Communications and Mobile Computing*, 2018. <https://doi.org/10.1155/2018/7107295>.
13. Andrews, J., Kowsika, M., Vakil, A., & Li, J. (2020a). A motion induced passive infrared (PIR) sensor for stationary human occupancy detection. In *2020 IEEE/ION position, location and navigation symposium (PLANS)*, pp. 1295–1304.
14. Andrews, J., Vakil, A., & Li, J. (2020b, December 5). Biometric authentication and stationary detection of human subjects by deep learning of passive infrared (PIR) sensor data. In *IEEE signal processing in medicine and biology (SPMB) 2020*.

15. Hobbie, R. K., & Roth, B. J. (2015). Intermediate physics for medicine and biology. In *Intermediate physics for medicine and biology* (5th ed.). Springer International Publishing. <https://doi.org/10.1007/978-3-319-12682-1>
16. Liu, X., Yang, T., Tang, S., Guo, P., & Niu, J. (2020b, April 16). From relative azimuth to absolute location. In *Proceedings of the 26th annual international conference on mobile computing and networking*. <https://doi.org/10.1145/3372224.3380878>.
17. Mukhopadhyay, B., Srirangarajan, S., & Kar, S. (2018). Modeling the analog response of passive infrared sensor. *Sensors and Actuators A: Physical*, 279. <https://doi.org/10.1016/j.sna.2018.05.002>.
18. Juan, R. O. S., Kim, J. S., Sa, Y. H., Kim, H. S., & Cha, H. W. (2016). Development of a sensing module for standing and moving human body using a shutter and PIR sensor. *International Journal of Multimedia and Ubiquitous Engineering*, 11(7). <https://doi.org/10.14257/ijmue.2016.11.7.05>.
19. University Receives \$1 Million for Transformational Energy Technology. (2018, January 23). *Stony brook matters: News for Alumni & Friends*. Retrieved from <https://news.stonybrook.edu/stony-brook-matters/alumni/university-receives-1-million-for-transformational-energy-technology/>
20. Wang, Y. (2020). *Current research projects*. Nanomaterial Energy Harvesting and Sensing (NES) Lab. Retrieved from <https://yawang08.wixsite.com/yawang/blank-c151z>.
21. Wu, L., Gou, F., Wu, S.-T., & Wang, Y. (2020). SLEEPIR: Synchronized low-energy electronically chopped PIR sensor for true presence detection. *IEEE Sensors Letters*, 4(3). <https://doi.org/10.1109/LESENS.2020.2976801>.
22. Wu, L., & Wang, Y. (2019). A low-power electric-mechanical driving approach for true occupancy detection using a shuttered passive infrared sensor. *IEEE Sensors Journal*, 19(1). <https://doi.org/10.1109/JSEN.2018.2875659>.
23. Wu, L., & Wang, Y. (2020, September 15). True presence detection via passive infrared sensor network using liquid crystal infrared shutters. In *ASME 2020 conference on smart materials, adaptive structures and intelligent systems*. <https://doi.org/10.1115/SMASIS2020-2366>.
24. Wu, L., Wang, Y., & Liu, H. (2018). Occupancy detection and localization by monitoring nonlinear energy flow of a shuttered passive infrared sensor. *IEEE Sensors Journal*, 18(21). <https://doi.org/10.1109/JSEN.2018.2869555>.
25. Shubhendu S., & Vijay, J. (2013). Applicability of artificial intelligence in different fields of life. *International Journal of Scientific Engineering and Research (IJSER)*, 1(1).
26. Topol, E. (2019). *Deep medicine*. Basic Books.
27. Hong, X., Gao, J., Jiang, X., & Harris, C. J. (2014). Estimation of Gaussian process regression model using probability distance measures. *Systems Science & Control Engineering*, 2(1). <https://doi.org/10.1080/21642583.2014.970731>.
28. Zhang, G., Wang, P., Chen, H., & Zhang, L. (2019a). Wireless indoor localization using convolutional neural network and gaussian process regression. *Sensors*, 19(11). <https://doi.org/10.3390/s19112508>.
29. Abiodun, O. I., Jantan, A., Omolara, A. E., Dada, K. V., Mohamed, N. A., & Arshad, H. (2018). State-of-the-art in artificial neural network applications: A survey. *Heliyon*, 4(11). <https://doi.org/10.1016/j.heliyon.2018.e00938>.
30. Shrestha, A., & Mahmood, A. (2019). Review of deep learning algorithms and architectures. *IEEE Access*, 7. <https://doi.org/10.1109/ACCESS.2019.2912200>.
31. Hochreiter, S. (1998). The Vanishing gradient problem during learning recurrent neural nets and problem solutions. *International Journal of Uncertainty, Fuzziness and Knowledge-Based Systems*, 6(2). <https://doi.org/10.1142/S0218488598000094>.
32. Adadi, A., & Berrada, M. (2018). Peeking inside the black-box: A survey on explainable artificial intelligence (XAI). *IEEE Access*, 6. <https://doi.org/10.1109/ACCESS.2018.2870052>.
33. Vakil, A. (2020). Heterogenous multimodal sensor fusion via canonical correlation analysis and explainable AI.

34. Li, D., Liu, J., Nishimura, S., Hayashi, Y., Suzuki, J., & Gong, Y. (2020a, October 12). Multi-person action recognition in microwave sensors. In *Proceedings of the 28th ACM international conference on multimedia*. <https://doi.org/10.1145/3394171.3413801>.
35. Singh, S., & Aksanli, B. (2019). Non-intrusive presence detection and position tracking for multiple people using low-resolution thermal sensors. *Journal of Sensor and Actuator Networks*, 8(3). <https://doi.org/10.3390/jsan8030040>.
36. Bianco, V., Mazzeo, P. L., Paturzo, M., Distante, C., & Ferraro, P. (2020). Deep learning assisted portable IR active imaging sensor spots and identifies live humans through fire. *Optics and Lasers in Engineering*, 124. doi:<https://doi.org/10.1016/j.optlaseng.2019.105818>.
37. Kim, S., Kang, S., Ryu, K. R., & Song, G. (2019). Real-time occupancy prediction in a large exhibition hall using deep learning approach. *Energy and Buildings*, 199. <https://doi.org/10.1016/j.enbuild.2019.06.043>.
38. Oguntala, G. A., Abd-Alhameed, R. A., Ali, N. T., Hu, Y.-F., Noras, J. M., Eya, N. N., Elfegani, I., & Rodriguez, J. (2019). SmartWall: Novel RFID-enabled ambient human activity recognition using machine learning for nonobtrusive health monitoring. *IEEE Access*, 7. <https://doi.org/10.1109/ACCESS.2019.2917125>.
39. Liu, J., Mu, H., Vakil, A., Ewing, R., Shen, X., Blasch, E., & Li, J. (2020a). Human occupancy detection via passive cognitive radio. *Sensors*, 20(15). <https://doi.org/10.3390/s20154248>.
40. Fan, L., Li, T., Fang, R., Hristov, R., Yuan, Y., & Katabi, D. (2020a, June). Learning longterm representations for person re-identification using radio signals. In *2020 IEEE/CVF conference on computer vision and pattern recognition (CVPR)*. <https://doi.org/10.1109/CVPR42600.2020.01071>.
41. Fan, L., Li, T., Yuan, Y., & Katabi, D. (2020b, August). In-home daily-life captioning using radio signals. In *European conference on computer vision (ECCV 2020)*.
42. Li, T., Fan, L., Zhao, M., Liu, Y., & Katabi, D. (2019, October). Making the invisible visible: Action recognition through walls and occlusions. In *2019 IEEE/CVF international conference on computer vision (ICCV)*. <https://doi.org/10.1109/ICCV.2019.00096>.
43. Singh, A. D., Sandha, S. S., Garcia, L., & Srivastava, M. (2019). RadHAR. In *Proceedings of the 3rd ACM workshop on millimeter-wave networks and sensing systems—MmNets'19*. <https://doi.org/10.1145/3349624.3356768>.
44. Zou, H., Zhou, Y., Yang, J., & Spanos, C. J. (2018). Towards occupant activity driven smart buildings via WiFi-enabled IoT devices and deep learning. *Energy and Buildings*, 177. <https://doi.org/10.1016/j.enbuild.2018.08.010>.
45. Das, A., Sangogboye, F. C., Raun, E. S. K. & Kjærgaard, M. B. HeteroSense: An Occupancy Sensing Framework for Multi-Class Classification for Activity Recognition and Trajectory Detection. in *Proceedings of the Fourth International Workshop on Social Sensing-SocialSense'19 (ACM Press, 2019)*. <https://doi:10.1145/3313294.3313383>.
46. Pham, M., Yang, D., & Sheng, W. (2019). A sensor fusion approach to indoor human localization based on environmental and wearable sensors. *IEEE Transactions on Automation Science and Engineering*, 16(1). <https://doi.org/10.1109/TASE.2018.2874487>.
47. Gochoo, M., Tan, T.-H., Velusamy, V., Liu, S.-H., Bayanduuren, D., & Huang, S.-C. (2017). Device-free non-privacy invasive classification of elderly travel patterns in a smart house using PIR sensors and DCNN. *IEEE Sensors Journal*. <https://doi.org/10.1109/JSEN.2017.2771287>.
48. Kashimoto, Y., Fujiwara, M., Fujimoto, M., Suwa, H., Arakawa, Y., & Yasumoto, K. (2017, March). ALPAS: Analog-PIR-sensor-based activity recognition system in smarhome. In *2017 IEEE 31st international conference on advanced information networking and applications (AINA)*. <https://doi.org/10.1109/AINA.2017.33>.
49. Wang, X., Wang, X., Mao, S., Zhang, J., Periaswamy, S. C. G., & Patton, J. (2020). Indoor radio map construction and localization with deep gaussian processes. *IEEE Internet of Things Journal*, 7(11). doi:<https://doi.org/10.1109/JIOT.2020.2996564>.
50. Zhang, G., Wang, P., Chen, H., & Zhang, L. (2019b). Wireless indoor localization using convolutional neural network and gaussian process regression. *Sensors*, 19(11). <https://doi.org/10.3390/s19112508>.

51. Zhang, B., Li, S., Huang, Z., Rahi, B. H., Wang, Q., & Li, M. (2018). Transfer learning-based online multiperson tracking with Gaussian process regression. *Concurrency and Computation: Practice and Experience*, 30(23). <https://doi.org/10.1002/cpe.4917>.
52. He, X., Aloï, D., & Li, J. (2016, January). Portable 3D visual sensor based indoor localization on mobile device. In *2016 13th IEEE annual consumer communications & networking conference (CCNC)*. <https://doi.org/10.1109/CCNC.2016.7444947>.
53. Burns, E., & Kakara, R. (2018). Deaths from falls among persons aged  $\geq 65$  years—United States, 2007–2016. *MMWR. Morbidity and Mortality Weekly Report*, 67(18). <https://doi.org/10.15585/mmwr.mm6718a1>.
54. Huang, Z., Liu, Y., Fang, Y., & Horn, B. K. P. (2018, October). Video-based fall detection for seniors with human pose estimation. In *2018 4th international conference on Universal Village (UV)*. <https://doi.org/10.1109/UV.2018.8642130>.
55. Kabelac, Z., Tarolli, C. G., Snyder, C., Feldman, B., Glidden, A., Hsu, C.-Y., Hristov, R., Dorsey, E. R., & Katabi, D. (2019). Passive monitoring at home: A pilot study in Parkinson disease. *Digital Biomarkers*, 3(1). <https://doi.org/10.1159/000498922>.
56. Vhaduri, S., & Poellabauer, C. (2019). Multi-modal biometric-based implicit authentication of wearable device users. *IEEE Transactions on Information Forensics and Security*, 14(12). <https://doi.org/10.1109/TIFS.2019.2911170>.
57. Hom Choudhury, S., Kumar, A., & Laskar, S. H. (2019). Biometric authentication through unification of finger dorsal biometric traits. *Information Sciences*, 497. <https://doi.org/10.1016/j.ins.2019.05.045>.
58. Clark, J. W., Neuman, M. R., Olson, W. H., Peura, R. A., Primiano, F. P., Siedband, M. P., Webster, J. G., & Wheeler, L. A. (2009). In J. G. Webster (Ed.), *Medical instrumentation: Application and design* (4th ed.). Wiley.
59. Zhang, Q. (2018, November). Deep learning of electrocardiography dynamics for biometric human identification in era of IoT. In *2018 9th IEEE annual ubiquitous computing, electronics & mobile communication conference (UEMCON)*. <https://doi.org/10.1109/UEMCON.2018.8796676>.
60. Wang, D., Si, Y., Yang, W., Zhang, G., & Liu, T. (2019). A novel heart rate robust method for short-term electrocardiogram biometric identification. *Applied Sciences*, 9(1). <https://doi.org/10.3390/app9010201>.
61. Li, Y., Pang, Y., Wang, K., & Li, X. (2020b). Toward improving ECG biometric identification using cascaded convolutional neural networks. *Neurocomputing*, 391. <https://doi.org/10.1016/j.neucom.2020.01.019>.
62. Xu, X., Liang, Y., He, P., & Yang, J. (2019). Adaptive motion artifact reduction based on empirical wavelet transform and wavelet thresholding for the non-contact ECG monitoring systems. *Sensors*, 19(13). <https://doi.org/10.3390/s19132916>.
63. Massaroni, C., Lo Presti, D., Formica, D., Silvestri, S., & Schena, E. (2019). Non-contact monitoring of breathing pattern and respiratory rate via RGB signal measurement. *Sensors*, 19(12). <https://doi.org/10.3390/s19122758>.
64. Li, F., Valero, M., Shahriar, H., Khan, R. A., & Ahamed, S. I. (2021). Wi-COVID: A COVID-19 symptom detection and patient monitoring framework using WiFi. *Smart Health*, 19. <https://doi.org/10.1016/j.smhl.2020.100147>.
65. Kapu, H., Saraswat, K., Ozturk, Y., & Cetin, A. E. (2017). Resting heart rate estimation using PIR sensors. *Infrared Physics & Technology*, 85. <https://doi.org/10.1016/j.infrared.2017.05.010>.
66. Lin, F., Song, C., Zhuang, Y., Xu, W., Li, C., & Ren, K. (2017, October 4). Cardiac scan. In *Proceedings of the 23rd annual international conference on mobile computing and networking*. <https://doi.org/10.1145/3117811.3117839>.